Silver Ion-Exchanged Zeolites Y, X, and Low-Silica X: Observations of Thermally Induced Cation/Cluster Migration and the Resulting Effects on the Equilibrium Adsorption of Nitrogen

Nick D. Hutson,[†] Barbara A. Reisner,[‡] Ralph T. Yang,*[,†] and Brian H. Toby[‡]

Department of Chemical Engineering, University of Michigan, Ann Arbor, Michigan 48109, and Center for Neutron Research, National Institute of Standards and Technology, Gaithersburg, Maryland 20899-8562

Received April 8, 2000. Revised Manuscript Received July 13, 2000

Silver is known to strongly affect the adsorptive properties of some zeolites. It is also known that thermal vacuum dehydration of some argentiferous zeolites leads to the formation of charged silver clusters within the zeolite. In this work we have synthesized silver zeolites of the types Y, X, and low-silica X. The zeolites were treated in such a way as to promote the formation of intracrystalline charged silver clusters. Equilibrium room-temperature isotherms were measured for adsorption of nitrogen for each of the zeolites after various heat treatments and dehydration. These materials were structurally characterized via Rietveld refinement using neutron powder diffraction data. Color changes upon heat treatment and subsequent X-ray photoemission spectroscopy confirmed some reduction of $Ag^+ \rightarrow Ag^0$. The effects of various dehydration conditions, including the time, temperature, and atmosphere, on the room-temperature adsorption of nitrogen are discussed. Structural characterization, along with valence bond calculations, revealed the presence of cations in site II*, which are more active in Ag−LSX samples that were vacuum dehydrated at 450 °C as compared to those that were vacuum dehydrated at 350 °C.

Introduction

Faujasite zeolites are composed of silica and alumina tetrahedra, which are joined together to form the truncated octahedral or sodalite structure and are connected with tertiary hexagonal prisms to form the structured zeolite unit cell. In these structures, the SiO_2 groups are electroneutral, but the $(AlO_2)^-$ groups are not, and thus introduce a negative charge to the structure that is offset by the presence of a charge-compensating, nonframework cation (e.g., Na^+, Li^+, Ca^{2+}). For the faujasite zeolites, the cation site designations are conventionally designated as SI (the center of the hexagonal prism), SI′ (opposite SI but located in the cuboctahedron), SII (single six-ring in the supercage), SII′ (opposite SII but inside the cuboctahedron), and SIII (near the four-ring windows in the supercage). The unit cell, including cation sites, for faujasite-type zeolites, is shown in Figure 1.

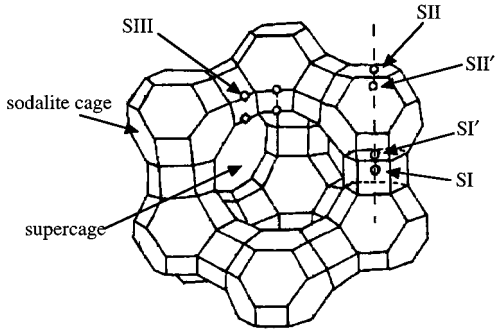

Figure 1. Unit cell, including cation sites, for faujasite zeolites.

It is known that the extraframework cations in the zeolite are largely responsible for the adsorptive capacity of these materials.[1,2] This is due primarily to van der Waals and Coulombic interactions between the charge-compensating cations of the zeolite and the adsorbing gas. Because the extraframework cations so significantly influence the adsorption properties of the zeolites, numerous attempts have been made to optimize these properties. This has been done (1) by increasing the number of cation sites (the cation exchange capacity, CEC) by creating zeolites with high aluminum content and (2) by synthesizing zeolites containing various combinations of alkaline metal and alkaline earth cations.

Kuhl reported a procedure for the synthesis of low-silica X-type zeolite (LSX). This material is an aluminum-saturated X-type zeolite with a silica-to-alumina ratio of 2.0 (or Si/Al = 1.0).[3] Commercial X zeolite, which is typically available as the Na^+ form (known commer-

* To whom correspondence should be addressed.
[†] University of Michigan.
[‡] National Institute of Standards and Technology.

(1) Barrer, R. M. *Zeolites and Clay Minerals as Sorbents and Molecular Sieves*; Academic Press: London, 1978.

(2) Breck, D. W. *Zeolite Molecular Sieves*; R. E. Krieger Publishing: Malabar, FL, 1984.

(3) Kuhl, G. H. *Zeolites* **1987**, *7*, 451.

10.1021/cm000294n CCC: $19.00
Published on Web 09/07/2000

cially as 13X), is not aluminum saturated and contains ≈86 aluminum atoms per unit cell, while the LSX zeolite contains 96 aluminum atoms per unit cell.

Silver is known to strongly influence the adsorption characteristics of some aluminosilicate zeolites. Habgood measured isotherms for N_2, O_2, C_2H_6, and C_2H_4 adsorbed on Ag−X zeolite and compared to those same gas isotherms measured on alkaline metal and alkaline earth cation-exchanged X zeolite.[4] The author noted that the alkaline metal and alkaline earth cations are all of a stable noble metal (closed shell) electronic configuration, whereas the d orbitals of the silver ion give it directional properties. The author concluded that the silver ion is more polarizing than the sodium ion, which has the same charge and a similar size. Huang measured adsorption of CO, N_2, O_2, CO_2, and C_2H_4 on Ag−X and Ag−Y zeolites.[5]

Yang et al. reported the synthesis of a mixed Li,Ag ion-exchanged X-type zeolite (Si/Al = 1.25 with approximately 17 Ag^+ per unit cell) and discussed its potential for use in adsorptive air separation.[6] This sorbent utilized the very strong adsorptive properties of the Ag^+ ion, which provided for increased capacity over that of the Li−X while maintaining some degree of the advantageous isotherm linearity that is seen with Li−X. Noting the high isosteric heat of adsorption for N_2 on Ag−X zeolites combined with a relatively slow desorption of N_2 on the same, the authors proposed some degree of weak π-complexation. The π-complexation character of the interaction was subsequently confirmed by ab initio molecular orbital calculations using N_2 and an Ag−X cluster model and was referred to as "weak chemisorption-assisted adsorption."[7] Hutson et al. have recently reported the synthesis of mixed Li,Ag low-silica X-type zeolite in which the addition of very small amounts of silver and specific dehydration conditions resulted in enhanced adsorptive characteristics and increased energetic heterogeneity relative to those of the near fully exchanged Li^+−zeolites.[8] Numerous attempts have been made to reduce transition metal ions in zeolites for the purpose of forming highly dispersed metallic clusters for use as catalysts. These attempts have typically been completed via treatment at elevated temperatures and/or in reducing atmospheres (e.g., sodium vapor, hydrogen gas, carbon monoxide gas). However, color changes upon vacuum dehydration of silver-exchanged A-type zeolites were found to be related to the formation of metallic clusters within the sodalite cage or the 6-prism of the zeolite.[9−11] Using volumetric sorption techniques and temperature-programmed desorption, Jacobs et al. were able to relate these color changes to an autoreductive process involving framework oxygen.[11] Autoreduction is the reduction of the transition metal ion and the oxidation of water or lattice oxygen. This has been observed for both Ag^+ and Cu^{2+} ions in zeolites A, X, and Y and has been shown to take place by two mechanisms in clearly defined temperature regions:[11,12]

(i) autoreduction in the presence of zeolite water (25−250 °C)

$$2(Ag^+{-}Z{-}O^-) + H_2O \rightarrow 2Ag^0 + (^1/_2)O_2 + 2Z{-}OH \quad (1)$$

and

(ii) autoreduction by oxygen from the zeolite lattice (127−380 °C)

$$2(Ag^+{-}Z{-}O^-) \rightarrow 2Ag^0 + (^1/_2)O_2 + Z{-}O^- + Z^+ \quad (2)$$

Kim and Seff proposed the formation of octahedral hexasilver metal clusters stabilized by coordination to six silver ions ($(Ag^+)_6(Ag)^6$) from structural determinations of a dehydrated silver-exchanged zeolite A.[9,10] However, Jacobs et al. suggested that the formation of such large metal clusters is improbable because color changes are seen even at low temperatures and low silver loadings where extensive migration of neutral silver atoms and subsequent sintering into Ag_6 metal clusters is highly unlikely. Alternatively, Jacobs et al. suggested, on the basis of structural studies of Ag−A zeolites, the formation of linear $(Ag_3)^{2+}$ charged clusters ($Ag^+{-}Ag^0{-}Ag^+$) upon thermal dehydration of the zeolite.[11]

Gellens et al. followed color changes and concomitant silver cluster formation in A, X, and Y zeolites using X-ray diffraction (XRD) techniques.[13−15] They found that the number of clusters increased with framework Al content. They also noted that, in synthetic analogues of the faujasite zeolite (types X and Y), the dehydrated zeolites displayed a yellow color, which increased in intensity with the number of clusters. However, silver-exchanged A zeolites took a yellow color with dehydration at low temperatures, eventually becoming brick red after treatment at higher temperatures. Further information can be found in a comprehensive review of silver clusters and chemistry in zeolites by Sun and Seff.[16]

The location of the extraframework silver in relation to the aluminosilicate framework is of primary importance for elucidating the effect of silver clustering on the adsorptive characteristics of the zeolite. This is not a trivial endeavor. Numerous studies have been undertaken to identify the location of Ag^+ ions and Ag clusters in argentiferous zeolites. These have mostly been for Ag−A and have included X-ray diffraction methods[9,10,13,14] and far-infrared spectroscopy.[12,17] It was found that, for dehydrated, fully Ag^+-exchanged faujasite-type zeolites, the silver molecules were distributed among the six-ring sites (SI, SI′, and SII for faujasites) and, for samples with high Al content, in the SIII

(4) Habgood, H. W. *Can. J. Chem.* **1964**, *42*, 2340.
(5) Huang, Y. *J. Catal.* **1974**, *32*, 482.
(6) Yang, R. T.; Chen, Y. D.; Peck, J. D.; Chen, N. *Ind. Eng. Chem. Res.* **1996**, *35*, 3093.
(7) Chen, N.; Yang, R. T. *Ind. Eng. Chem. Res.* **1996**, *35*, 4020.
(8) Hutson, N. D.; Rege, R. U.; Yang, R. T. *AIChE J.* **1999**, *45*, 724.
(9) Kim, Y.; Seff, K. *J. Am. Chem. Soc.* **1978**, *100*, 175.
(10) Kim, Y.; Seff. K. *J. Am. Chem. Soc.* **1978**, *100*, 6989.
(11) Jacobs, P. A.; Uytterhoeven, J. B.; Beyer, H. K. *J. Chem. Soc., Faraday Trans.* **1979**, *75*, 56.
(12) Baker, M. D.; Ozin, G. A.; Godber, J. *J. Phys. Chem.* **1985**, *89*, 305.
(13) Gellens, L. R.; Mortier, W. J.; Schoonheydt, R. A.; Uytterhoeven, J. B. *J. Phys. Chem.* **1981**, *85*, 2783.
(14) Gellens, L. R.; Mortier, W. J.; Uytterhoeven, J. B. *Zeolites* **1981,** *1*, 11.
(15) Gellens, L. R.; Smith, J. V.; Pluth, J. J. *J. Am. Chem. Soc.* **1983**, *105*, 51.
(16) Sun, T.; Seff, K. *Chem. Rev.* **1994**, *94*, 857.
(17) Ozin, G. A.; Baker, M. D.; Godber, J. *J. Phys. Chem.* **1984**, *88*, 4902.

locations. Gellens et al.[14] and Baker et al.[12] showed the simultaneous occupancy of sites SI and SI′ by linear ($Ag^+-Ag^0-Ag^+$) clusters.

In this work we have synthesized Ag^+ ion-exchanged zeolites and treated these materials in ways that promote the formation of intracrystalline silver clusters. Extraframework silver cations were located through Rietveld refinement using neutron diffraction data. The nitrogen adsorptive characteristics of these materials were evaluated with respect to the position and coordination of their extraframework cations through structural information and valence bond calculations.

Experimental Details

Materials. The zeolites used in this work, LSX zeolite (Si/Al =1.0, Praxair, No. 16193-42), X zeolite (Si/Al = 1.25, Linde, Lot 945084060002), and Y zeolite (Strem, Lot 128671-S), were obtained from commercial sources as binderless, hydrated powders and were used as received. Silver nitrate ($AgNO_3$, 99.9%, Strem) was used in the preparation of ion-exchange solutions. Deionized water was used for the preparation of all ion-exchange solutions and for sample washing. Helium (99.995%) and nitrogen (99.998%) were obtained from Cryogenic Gases and were used for isotherm adsorption measurements without further purification.

Synthesis of Silver-Exchanged Faujasites. The silver zeolites were prepared using standard ion-exchange methods. A zeolite sample was exchanged by contacting the material two times with a 0.5 M aqueous $AgNO_3$ solution. In other studies, we have also used Ag−acetate as the silver source, but found that the resulting Ag−zeolites were the same, with respect to their adsorptive characteristics, as those from the $AgNO_3$ solution. Each silver solution contained a cation content that was in 2-fold excess of what was required to achieve 100% exchange. There was no effort made to control the pH of the solution; however, there was no visible precipitation prior to addition of the zeolite. The ion-exchange solution was heated to a mild boil with constant agitation and immediately allowed to cool and settle. After the first ion exchange, the solution was decanted, fresh solution was added, and the mixture was reheated. After the second ion exchange, the material was vacuum filtered and washed with copious amounts of water until no precipitate was seen upon treatment with free chloride. The silver-exchanged samples were dried at room temperature and atmospheric conditions in a dark area. The resulting materials were dehydrated prior to analysis, as described below.

Sample Dehydration. Zeolites have a strong affinity for water, and some molecules are tenaciously held. The presence of adventitious water will affect the cation coordination in the zeolites, as determined through powder diffraction analysis, and the adsorption of guest molecules, as measured by adsorption isotherms. Furthermore, dehydration conditions strongly influence the formation of silver clusters. To separate these effects, the atmosphere, temperature, and length of time of dehydration were rigorously controlled.

Temperature. Samples of Ag−Y, Ag−X, and Ag−LSX were dehydrated under vacuum at temperatures ranging from 100 to 600 °C at times ranging from 1 to 24 h. The samples were heated at ≈20 °C/min to "hold points" in 100 °C intervals, and then the samples were held for ≈30 min before being ramped up to the next hold point. When the sample was raised to the desired final dehydration temperature, it was soaked at that temperature for a specified amount of time and then allowed to cool to room temperature with no further applied heating. Throughout this paper, samples are referred to as Ag−M−N, where M specifies the identity of the zeolite (X, Y, or LSX) and N denotes the dehydration temperature.

Time. To determine the effect of dehydration time on cluster formation and the resulting adsorptive characteristics of Ag−LSX, a sample was vacuum dehydrated at 450 °C for varying amounts of times, and the resulting N_2 adsorption isotherms were measured.

Atmosphere. The effects of the dehydration atmosphere were determined by controlling both the sample drying and dehydration. Samples were treated in the following ways: (1) dried in a dark area at room temperature and then dehydrated under vacuum for 4 h at 450 °C, (2) dried in a standard convection oven at 100 °C in air and then dehydrated under vacuum for 4 h at 450 °C, and (3) heated slowly (<10 °C/min) in a furnace to 450 °C in air and then dehydrated under vacuum for 4 h at 450 °C.

Neutron Activation Analysis. Chemical analysis was performed by neutron activation analysis (NAA) at the research nuclear reactor of the Phoenix Memorial Laboratory at the University of Michigan. The samples were irradiated sequentially for 1 min at a core-face location with an average thermal neutron flux of 2×10^{12} n/cm^2/s. Two separate γ-ray spectra were collected for 500-s real time for each sample using a high-resolution germanium detector. The collection after a 13-min decay was used to determine the concentrations of aluminum and silver, while data collected after1 h and 56 min of decay were used to analyze for sodium and potassium. Four replicates of NBS-SRM-1633a (coal fly ash) and silver foil were used as standard reference materials and check standards.

Adsorption Isotherm Measurements. The adsorption isotherms were measured, normally at 25 °C, using a static volumetric system (Micromeritics ASAP-2010). Additions of the adsorbate gas were made at volumes required to achieve a targeted set of pressures. A minimum equilibrium interval of 5 s with a tolerance of 5% of the target pressure (or 5 Torr, whichever is smaller) was used to determine equilibrium for each measurement point.

X-ray Photoemission Spectroscopy. X-ray photoemission spectra were obtained from thin wafers of the zeolites using a Perkin-Elmer PHI 5400 ESCA system with a Mg anode. An absence of surface charging was verified by measuring the binding energy of adventitious carbon. The generally accepted reference for the binding energy of C 1s photoelectrons is 285 ± 0.2 eV.[18]

Samples of fully exchanged Ag−LSX zeolite, which were (1) fully hydrated, (2) heated in a vacuum at 200 °C, and (3) heated in a vacuum at 450 °C, were formed into very thin wafers using a laboratory press. The wafers were then degassed in the XPS staging cell at $10^{-8}-10^{-9}$ Torr for 2 days at room temperature prior to analysis.

Powder Neutron Diffraction Data Collection. Powder neutron diffraction data were collected for Ag−Y-450, Ag−X-450, Ag−LSX-350, and Ag−LSX-450. Each of the samples was initially dehydrated under vacuum for 12 h, as described in the sample dehydration protocol. The samples were exposed to atmospheric conditions during transport to the NIST Center for Neutron Research (NCNR). In preparation for the diffraction experiment, roughly 10−15 mL of each sample was dehydrated under vacuum (<10^{-5} Torr). Each sample was heated to the temperature that had been used in the prior heat treatment. Samples were heated at a rate of ≈10 °C/min, held at constant temperature for a minimum of 4 h, and then allowed to cool to room temperature. The samples were transferred to 50-mm long and 15.6-mm wide vanadium cans and subsequently sealed in a helium environment with low water and oxygen levels (<10 ppm).

Neutron diffraction data were collected using the 32 detector BT-1 neutron powder diffractometer at the NIST Center for Neutron Research NBSR reactor. Measurements were made using a Ge(311) monochromator with $\lambda = 2.0783(2)$ Å (1 Å = 10^{-10} m) at ambient temperature. Data were collected over the range of 1.3−166.3° 2θ with a step size of 0.05°. The data collection time for each sample was ≈8 h. The BT-1 instrument is described at the NCNR WWW site (http://www.ncnr.nist.gov/).

(18) Briggs, B.; Shea, M. P. *Practical Surface Analysis. Volume 1. Auger and X-ray Photoemission Spectroscopy*; John Wiley and Sons: New York, 1990; p 543.

Table 1. Unit Cell Composition (in atoms/unit cell (uc)) for Silver-Exchanged Faujasites

compd	Ag−LSX atoms/uc	Ag−X atoms/uc	Ag−Y atoms/uc
Al	96.0	86.0	56.0
Ag	112.5	98.2	59.6
Na	0.2	0.4	2.4
Si	96.0	106.0	136.0
O	384.0	384.0	384.0

Table 2. Heat Treatment Conditions and Resulting Color Changes for Ag-Zeolites

zeolite	heat treatment	color change
Ag−Y	initial	white
	200 °C in vac, 4 h	slightly gray
	450 °C in vac, 4 h	dark gray
Ag−X	initial	gray
	160 °C in vac, 1 h	gray tan
	250 °C in vac, 1 h	pale yellow
	350 °C in vac, 1 h	yellow
	450 °C in vac, 1 h	golden yellow
	450 °C in vac, 4 h	deep golden yellow
Ag−LSX	initial	gray
	100 °C in vac, 24 h	gray
	200 °C in vac, 4 h	brownish yellow
	300 °C in vac, 4 h	yellow
	350 °C in vac, 4 h	golden yellow
	450 °C in vac, 4 h	deep golden yellow

Results and Discussion

Chemical Analysis. The unit cell compositions for each of the materials studied are listed in Table 1. Each of the analyzed zeolites had a silver content in excess of the expected value based upon aluminum analysis. This is mostly likely due to the presence of silver metal particles present on the outside surface of the zeolite crystallites. This phenomenon has been previously noted in other Ag^+-exchanged members of the faujasite family.[14] In retrospect, considering the ease of the exchange of Ag^+ into zeolites and the tendency for Ag^+ to reduce, milder ion-exchange conditions (e.g., no heating) could have been used. Future researchers should take this into consideration. Also, all ion exchanges were performed in the presence of light, and although the samples were stored in a dark area and the heat treatment and adsorption measurements were performed with minimal light, this could also have contributed to the presence of metallic silver in the samples.

Effect of Sample Preparation on Nitrogen Adsorption. Dehydration conditions, particularly the atmosphere, duration, and dehydration temperature used, strongly influence the formation of the silver clusters.[9,10,13,14] The effect of the dehydration conditions on extraframework silver can be assessed by looking at the effects of dehydration treatment on sample color and nitrogen adsorption.

Temperature Effects. Color changes upon vacuum dehydration of silver-exchanged A-type zeolite were found to be related to the formation of metallic clusters within the sodalite cage or the 6-prism of the zeolite.[9−11] These color changes are also evident in X-type zeolite. A summary of some dehydration conditions and the resulting color changes in the zeolites of interest in this study are given in Table 2. The Ag−X and Ag−LSX behaved very similarly, both becoming deep golden yellow with thermal vacuum dehydration. Gellens et al. observed that the yellow color occurred in Ag−A when, on average, only one cluster per sodalite cage was formed.[13,14] The Ag−X and Ag−LSX zeolites maintain the yellow color because there is no interaction between silver clusters. These authors also noted that more Ag present in the faujasite-type zeolite resulted in brighter color upon thermal vacuum dehydration.

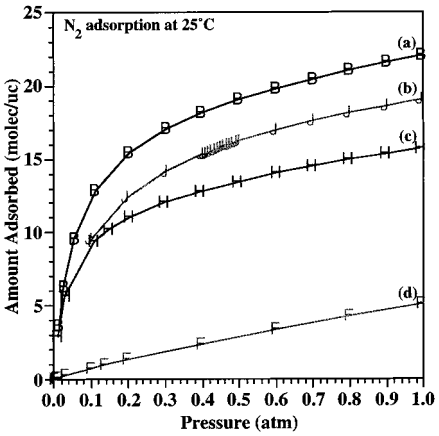

Figure 2. N_2 adsorption isotherms, measured at 25 °C, for (a) Ag−LSX-450 (vacuum dehydrated at 450 °C), (b) Ag−LSX-350 (vacuum dehydrated at 350 °C), (c) Ag−X, and (d) Ag−Y.

Effects of Dehydration Temperature. To determine the effect of temperature on silver cluster formation and the subsequent adsorptive characteristics, samples of the air-dried Ag−LSX zeolite were heated to various temperatures in a vacuum. The room-temperature N_2 adsorption isotherm was then measured for each of the heat-treated materials. The results are shown in Figure 2. In this plot the Ag−LSX sample shows a considerable increase in N_2 capacity after dehydration at 450 °C over that of the same sample dehydrated at 350 °C (at 25 °C and 1 atm, 22 molecules of N_2 and 19 molecules of N_2 per unit cell, respectively). This increase cannot be attributed to a loss of water because all but the most tenaciously held water is removed by 350 °C,[2] and there is no increase in the N_2 capacity for other zeolite forms (Li^+, Na^+, K^+, etc.) with dehydration at temperatures beyond 350 °C. Ag−LSX zeolites, which had been dehydrated in a vacuum at 550 and 600 °C, had N_2 capacities that were considerably lower than those dehydrated in a vacuum at 450−500 °C. Similarly, N_2 adsorption isotherms were measured for the Ag−X zeolites after thermal vacuum dehydration at 350 and 450 °C. This sample did not show the same increase in N_2 adsorption capacity with the higher temperature dehydration (at 1 atm, both samples adsorbed ≈15.5 molecules of N_2 per unit cell).

Effects of Duration of Dehydration. Migration of silver ions, most likely to or from the sodalite cage and hexagonal prism, and possibly from one unit cell to another, is necessary to form the charged metallic clusters. Using a theoretical model of diffusion into a sphere, Cvjeticanin and Petranovic showed that the diffusion of Ag^+ is the rate-determining step in silver cluster formation.[19] To determine the effect of dehydration time on cluster formation, and the resulting adsorptive characteristics, the Ag−LSX sample was vacuum dehydrated at 450 °C at various times and the resulting N_2 adsorption isotherms were measured. These are shown in Figure 3. From these results one can see that

(19) Cvjeticanin, N. D.; Petranovic, N. A. *Zeolites* **1994**, *14*, 35.

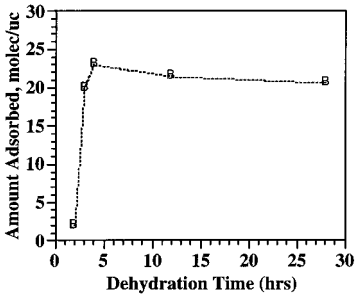

Figure 3. Amount of N_2 adsorbed at 25 °C and 1 atm versus dehydration time for Ag−LSX. All samples were vacuum dehydrated at 500 °C.

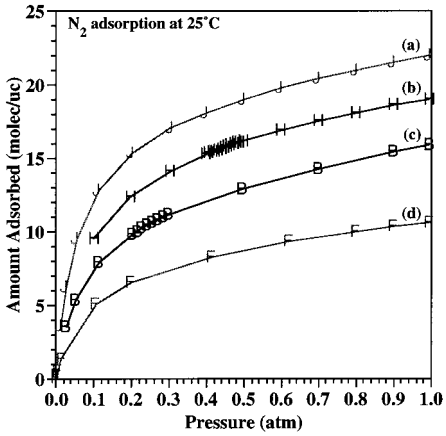

Figure 4. N_2 adsorption isotherms, measured at 25 °C, for Ag−LSX (a) after drying at room temperature followed by vacuum dehydration at 450 °C, (b) after drying at room temperature followed by vacuum dehydration at 350 °C, (c) after drying in air at 100 °C followed by vacuum dehydration at 350 °C, and (d) after drying in air at 100 °C in air followed by heat treatment in air at 450 °C and finally vacuum dehydration at 450 °C.

the N_2 adsorption capacity increased sharply between 2 and 3 h of dehydration and finally peaked at about 4 h. No further enhancement of the adsorption capacity was seen after the peak at 4 h. The initial sharp increase in the adsorptive capacity was due to loss of water in the zeolite. Because of this, all subsequent samples were dehydrated for a minimum of 4 h (but usually longer).

Effects of Dehydration Atmosphere. Because the formation of charged silver clusters is a reductive process, the presence of gaseous oxygen during the dehydration process is expected to hinder the autoreduction reaction. To evaluate this, samples of the Ag−LSX zeolites were dehydrated in the following ways: (1) allowed to dry in a dark area at room temperature (≈25 °C) before vacuum dehydration at 450 °C, (2) dried in a standard convection oven at 100 °C in air before being vacuum dehydrated at 450 °C, and (3) heated slowly in air in a furnace to 450 °C before being heated in a vacuum to 450 °C. The isotherms for adsorption of N_2 on each of the resulting materials are shown in Figure 4. One can see that any heating in air results in a reduction in the ultimate adsorptive capacity of the Ag−zeolite, and heating to a high temperature (i.e., to 450 °C) in air resulted in a considerable reduction in the ultimate adsorptive capacity as compared to that of the material that was dried at room temperature and dehydrated entirely in a vacuum. Samples of the Ag−X zeolite were also dehydrated using methods (1) and (2) as described

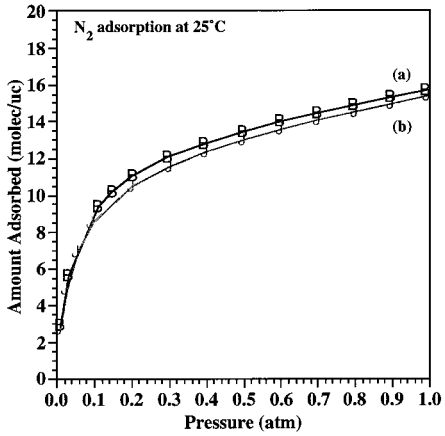

Figure 5. N_2 adsorption isotherms, measured at 25 °C, for Ag−X (a) after drying at room temperature followed by vacuum dehydration at 450 °C and (b) after drying in air at 100 °C followed by vacuum dehydration at 350 °C.

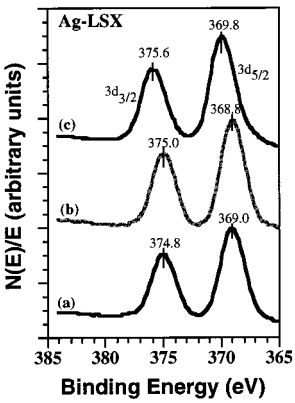

Figure 6. X-ray photoemission spectroscopy (XPS) spectra for Ag−LSX. The spectra were collected after (a) no thermal treatment, (b) heating at 200 °C in a vacuum, and (c) heating at 450 °C in a vacuum.

above and are shown in Figure 5. Contrary to the Ag−LSX results, there was little difference in the adsorptive capacity of these samples (both adsorbed ≈15.5 molecules of N_2 per unit cell at 1 atm).

XPS Analysis. X-ray photoemission spectroscopy (XPS or ESCA) is a surface analysis tool that is commonly used because of its ability to identify chemical states of atoms based on shifts of core-level binding energies. While most studies of silver systems indicate an anomalous negative shift in binding energy (BE) of the Ag 3d peaks as the oxidation state is increased, other studies show no BE shift with increasing oxidation state.[20] Even in cases where there has been a reported binding energy shift, shifts tend to be small (0.1−0.8 eV), which further complicates the interpretation of the spectra.

The Ag 3d peaks obtained from the Ag−LSX zeolite samples are shown in Figure 6. The observed Ag 3d binding energies for the silver zeolites and some other silver compounds are listed in Table 3. As a hydrated Ag−LSX sample is taken from room temperature to 450 °C, there is an observable negative shift in the binding energy as referenced to the Fermi level. This shift is suggestive of some reduction of the silver cations in the zeolite during the vacuum heating process. Any reduced

(20) Wolan, J. T.; Hoflund, G. B. *Appl. Surf. Sci.* **1998**, *125*, 251.

Table 3. Binding Energies (eV) for Silver Zeolites and Other Silver Compounds of Interest

material	BE ($3d_{5/2}$)	BE ($3d_{3/2}$)	ΔBE
Ag−LSX (hydrated)	369.0	374.8	5.8
Ag−LSX (200 °C vac)	368.8	375.0	6.2
Ag−LSX (450 °C vac)	369.8	375.6	5.8
Ag metal[30]	367.9	373.9	6.0
Ag_2O[31]	367.8	373.8	6.0
AgF[20]	367.8	373.7	5.9
AgF_2[20]	367.3	373.4	6.1

Ag present in the zeolite prior to heat treatment would not be observed because we are only able to infer Ag reduction by the shift in the binding energy when compared to a reference. We do not have a reference for the unheated sample. While this shift is an indication of silver reduction in the sample, the source of the silver could be either extraframework charge-compensating cations or the excess surface silver that has been postulated for these materials (though the excess surface silver is likely already reduced prior to vacuum heating). Nevertheless, the results indicate that there is reduction of some of the silver present in the Ag−LSX sample upon vacuum dehydration.

Structural Characterization of Ag-Exchanged Faujasites. Neutron powder diffraction data were analyzed using the Rietveld technique in conjunction with the GSAS (generalized structure analysis system) suite of Larson and Von Dreele.[21,22] To determine the best expected fit to the data, the LeBail intensity extraction method was first used, in effect simulating a fit with an idealized crystallographic model.[23] Background was fit using a Chebychev polynomial with 8 to 12 terms. Lattice constants and zero point shifts were simultaneously optimized. The peak asymmetry at low angles was treated using the model of Finger et al.[24,] Scattering lengths were set to standard values for neutral atoms, as supplied in the GSAS package.

Initial fractional atomic coordinates for the framework constituents in space group $Fd\bar{3}$ (203) were based upon the model determined by Feuerstein and Lobo for Li−LSX.[25] For X and Y, T(1) is treated as a pure Si site, while the T(2) site contains both Al and Si with fractional occupancies fixed in accordance with chemical analysis. The positions and thermal parameters of aluminum and silicon on T(2) were constrained to be identical. Soft constraints in the form of preferred interatomic distances were used to supplement the observed data, with Si−O distances set to the sum of their ionic radii (1.62 ± 0.01 Å) and T(2)−O distances set to the weighted average, based upon chemical analysis, of the sum of the Al−O and Si−O atomic radii (1.684, 1.719, and 1.73 Å ± 0.01 Å for Y, X, and LSX respectively).[26] During the final stages of refinement, soft constraints were reduced to minimal levels but could not be removed. The isotropic atomic displacement parameters were grouped, using one value for framework T atoms, a second value for framework O atoms, and a third for extraframework species.

Table 4. Cell Parameters and Agreement Factors for the Four Silver-Exchanged Faujasite Samples (The Agreement Factors for Each Crystallographic Model Is Compared to an Ideal (Le Bail) Fit; Definitions for R_{wp} and χ^2 Can Be Found in Ref 32 and $R_{Bragg} = \sum|F_o^2 - F_c^2|/\sum F_o^2$

parameter	Ag−Y-450	Ag−X-450	Ag−LSX-350	Ag−LSX-450
space group	$Fd\bar{3}$ (203)	$Fd\bar{3}$ (203)	$Fd\bar{3}$ (203)	$Fd\bar{3}$ (203)
$a = b = c$ (Å)	24.8730(2)	25.2013(3)	25.1534(7)	25.1126(7)
R_{wp} (Le Bail)	0.0455	0.0483	0.0476	0.0481
χ^2 (Le Bail)	1.173	1.313	1.053	1.195
R_{wp} (Rietveld)	0.0556	0.0579	0.0826	0.0845
R_{Bragg} (Rietveld)	0.0463	0.0493	0.0584	0.0585
χ^2 (Rietveld)	1.766	1.884	1.599	1.534
soft constraint contribution to χ^2	2.3 %	0.95 %	1.7 %	0.73 %

Details describing the determination of extraframework cation positions for each material are given in the following sections. The refinement parameters are summarized in Table 4. Atomic coordinates, site occupancies, and atomic displacement parameters are given in Table 5, with selected bond distances and angles given in Tables 6 and 7. A comparison of the silver site occupancies in silver-exchanged faujasites is given in Table 8. Figure 7 shows the final observed and calculated diffraction profiles for these materials.

Ag−Y-450. Following the refinement of the framework species, the positions and occupancies of the silver cations were examined. Silver cations were found entirely in the six-ring sites. As expected, no silver cations were observed in the SIII (supercage) site. The structural model contains four different Ag sites: in the center of the hexagonal prism connecting the sodalite cages (I), near the six-ring window of this prism on the inside of the sodalite cage (I′), and on either side of the single six-ring windows between the sodalite cage and supercage (II and II′). These cation sitings with relation to the sodalite cages are shown in Figure 8.

Simultaneous occupancy of cations at sites II and II′ is unlikely due to Coulombic repulsion between cations occupying these sites. Fractional occupancies of cations on these sites were constrained so that their sum was unity because their occupancies tended to refine to slightly larger totals. Most silver cations were found at the site II position, 85.9%, while the remainder were located at the II′ site. The remaining silver cations were distributed between the I and I′ sites with fractional occupancies refining to ≈68 and 39%, respectively. We feel that the standard uncertainty values from the least-squares refinement significantly underestimate the true errors in the fractional occupancies. The values of the fractional occupancies correlate with the displacement parameters; artificially raising or lowering the displacement parameters by a factor of 2 typically results in a change in the fractional occupancy by about 10%. The total occupancies for I and I′ were not constrained and these numbers total close enough to unity to lead us to believe that simultaneous occupancy of these sites does not occur in Ag−Y. This, along with the observation that the Ag−Y-450 sample never took the characteristic golden yellow color, makes it unlikely that this sample contained silver clusters.

(21) Rietveld, H. M. *Acta Crystallogr.* **1967**, *22*, 151.
(22) Larson, A. C.; van Dreele, R. B. *GSAS: General Structure Analysis System Manual*; Los Alamos Report LAUR 86-748; Los Alamos National Laboratory: Los Alamos, NM, 1986.
(23) Le Bail, A.; Duroy, H.; Fourquet, J. L. *Mater. Res. Bull.* **1988**, *23*, 447.
(24) Finger, L. W.; Cox, D. E.; Jephcoat, A. P. *J. Appl. Crystallogr.* **1994**, *27*, 892.
(25) Feuerstein, M.; Lobo, R. F. *Chem. Mater.* **1998**, *10*, 2197.
(26) Shannon, R. D.; Prewitt, C. T. *Acta Crystallogr* **1969**, *B25*, 925.

Table 5. Final Atomic Parameters for Fully Silver Exchanged Faujasites Refinements Using Neutron Powder Diffraction Data with Standard Uncertainties in Parentheses

atom	site		Ag−Y-450	Ag−X-450	Ag−LSX-350	Ag−LSX-450
T(1)[a]	96g	*x*	−0.0542(3)	−0.0521(2)	−0.0510(4)	−0.0484(3)
		y	0.1238(4)	0.1258(4)	0.1230(4)	0.12301(4)
		z	0.0336(3)	0.0323(3)	0.0326(4)	0.0321(3)
		B (Å^2)[b]	0.0060(8)	0.012(1)	0.017(2)	0.019(2)
T(2)[a]	96g	*x*	−0.0558(3)	−0.0557(3)	−0.0546(4)	−0.0558(3)
		y	0.0375(3)	0.0396(3)	0.0393(4)	0.0408(3)
		z	0.1240(4)	0.1216(3)	0.1233(4)	0.1227(3)
O(1)	96g	*x*	−0.1098(3)	−0.1093(3)	−0.1100(4)	−0.1102(3)
		y	0.0046(3)	0.0014(4)	0.0057(4)	0.0055(4)
		z	0.1046(3)	0.1045(3)	0.1009(4)	0.0993(4)
		B (Å^2)[b]	0.021(5)	0.0242(6)	0.026(1)	0.026(1)
O(2)	96g	*x*	−0.0045(3)	−0.0043(2)	−0.0038(4)	−0.0051(3)
		y	−0.0011(3)	−0.0006(2)	−0.0015(4)	0.0001(3)
		z	0.1416(2)	0.1408(2)	0.1453(3)	0.1454(3)
O(3)	96g	*x*	−0.0348(2)	−0.0338(2)	−0.0324(3)	−0.0309(3)
		y	0.0725(3)	0.0749(3)	0.0711(4)	0.0709(3)
		z	0.0698(3)	0.0676(3)	0.0666(4)	0.0660(3)
O(4)	96g	*x*	−0.0676(2)	−0.0690(2)	−0.0693(3)	−0.0693(4)
		y	0.0768(3)	0.0778(3)	0.0798(4)	0.0810(4)
		z	0.1769(3)	0.1764(3)	0.1771(4)	0.1772(4)
Ag(I)	16c	*x*=*y*=*z*	0	0	0	0
		occ.	0.68(2)	0.13(2)	0.53(3)	0.53(3)
		B (Å^2)[b]	0.0209(5)	0.015(2)	0.045(4)	0.054(4)
Ag(I′)	32e	*x*=*y*=*z*	0.0560(4)	0.0541(5)	0.0611(4)	0.0641(4)
		occ.	0.39(1)	0.43(2)	0.73(2)	0.72(3)
Ag(I′b)	32e	*x*=*y*=*z*		0.0303(4)		
		occ.		0.44(2)		
Ag(II′)	32e	*x*=*y*=*z*	0.1828(13)			
		occ.	0.14(1)			
Ag(II)	32e	*x*=*y*=*z*	0.2293(2)	0.2207(4)	0.2177(9)	0.2182(4)
		occ.	0.86(1)	0.81(2)	0.79(3)	0.78(2)
Ag(II*)	32e	*x*=*y*=*z*		0.238(2)	0.240(2)	0.247(2)
		occ.		0.19(3)	0.21(3)	0.22(2)
Ag(III)	96g	*x*		0.357(2)	0.352(3)	0.254(3)
		y		0.360(2)	0.355(3)	0.356(3)
		z		0.141(1)	0.148(2)	0.152(2)
		occ.		0.16(1)	0.20(1)	0.21(1)
Al(ALUM)	8a	*x*		0.125	0.125	0.125
		occ.		0.18(1)	0.27(1)	0.38(2)
O(ALUM)	32e	*x*		0.1646(1)	0.1650(1)	0.169(1)
		occ.		0.18(1)	0.27(1)	0.38(2)

[a] The T(1) site is completely occupied by Si. The composition of the T(2) site is fixed according to elemental analysis data obtained from NAA.

Ag−Y-450	Al = 0.583	Si = 0.417
Ag−X-450	Al = 0.896	Si = 0.104
Ag−LSX-350	Al = 1.000	Si = 0.000
Ag−LSX-450	Al = 1.000	Si =0.000

[b] Displacement parameters were fixed for each refinement as follows: T(1) = T(2), O(1) = O(2) = O(3) = O(4), Ag(I) = Ag(I′) = Ag(I″) = Ag(II′) = Ag(II′) = Ag(III) = Al(ALUM) = O(ALUM).

During the final cycles of refinement, soft constraints contributed a relatively large amount, 2.3%, to the total of χ^2. This is necessary because the large amount of silicon on T(2) makes the site practically indistinguishable from T(1). Silver occupancies total slightly lower than the amount expected from the framework composition, but are within the expected error.

Ag−X-450. The initial silver cation positions were those obtained for Ag−Y with additional silver placed in site III from a previously determined structure of Ag−X.[14] Fourier difference analysis indicated the presence of a significant amount of scattering density at the center of the sodalite cage and ≈1.7 Å away from this site. We initially attempted to model this as an occluded Ag species (such as precipitated $Ag(OH)_x$). However, all efforts to encourage these results using Rietveld refinement were unsuccessful. Another possible explanation for this extra scattering density is the presence of extraframework alumina in the center of the sodalite cage. Even when carefully dehydrated, X and LSX tend to lose framework alumina through self-steaming to void spaces in the zeolite (the sodalite cage and supercage). An extraframework tetrahedral $[AlO_4]^-$ unit was added to the model with the Al^{3+} located at the center of the sodalite cage and oxygen atoms along the (111) axis. The fractional occupancies for these two atoms were constrained to be the same. Isotropic atomic displacement parameters were constrained to be the same as that of the extraframework silver. Soft constraints were placed on the Al−O bond distance (1.73 Å) to maintain chemically reasonable Al−O bond lengths.

After vacuum dehydration the Ag−X-450 turned a golden yellow color that has been attributed to the formation of silver clusters at the hexagonal prism.[14] Difference Fourier analysis revealed the presence of additional scattering density on either side of this initial I′ site. There is evidence for either significant anisotropy at this site, and at all other sites along the (111) axis (*x*

Table 6. Selected Interatomic Distances (Å) and Bond Angles (°) Derived from Fully Silver Exchanged Faujasites with Standard Uncertainties in Parentheses

atoms	Ag−Y-450	Ag−X-450	Ag−LSX-350	Ag−LSX-450
T(1)−O(1)	1.610(8)	1.625(6)	1.616(9)	1.622(7)
T(1)−O(2)	1.686(11)	1.637(8)	1.644(15)	1.635(11)
T(1)−O(3)	1.634(8)	1.626(4)	1.629(7)	1.624(4)
T(1)−O(4)	1.608(8)	1.621(4)	1.625(7)	1.627(4)
⟨T(1)−O⟩	1.63			
T(2)−O(1)	1.645(7)	1.714(3)	1.724(7)	1.730(4)
T(2)−O(2)	1.656(8)	1.715(3)	1.730(7)	1.729(4)
T(2)−O(3)	1.688(8)	1.718(3)	1.730(7)	1.730(4)
T(2)−O(4)	1.665(8)	1.716(3)	1.734(10)	1.734(4)
⟨T(2)−O⟩	1.66			
Al(ALUM)−O(ALUM)		1.730(4)	1.741(3)	1.93(4)
O(1)−T(1)−O(2)	109.5(6)	114.1(6)	109.0(7)	108.9(6)
O(1)−T(1)−O(3)	112.7(6)	108.3(7)	111.9(7)	110.9(7)
O(1)−T(1)−O(4)	111.4(6)	107.9(5)	107.5(8)	104.7(7)
O(2)−T(1)−O(3)	106.5(6)	105.3(6)	110.2(8)	112.0(7)
O(2)−T(1)−O(4)	107.8(6)	113.8(5)	108.2(7)	110.9(6)
O(3)-T(1)-O(4)	108.8(5)	107.0(5)	109.9(7)	109.3(7)
⟨O−T(1)-O⟩				
O(1)−T(2)−O(2)	114.6(6)	109.5(5)	114.2(7)	113.1(6)
O(1)−T(2)−O(3)	106.0(6)	110.1(6)	102.5(7)	103.3(6)
O(1)−T(2)−O(4)	112.4(6)	111.3(5)	111.8(8)	114.4(7)
O(2)−T(2)−O(3)	105.8(6)	106.6(5)	107.4(7)	105.2(6)
O(2)−T(2)−O(4)	105.5(6)	104.7(6)	104.9(7)	103.1(6)
O(3)−T(2)−O(4)	112.5(5)	114.2(5)	116.2(7)	117.7(6)
⟨O−T(2)−O⟩				
T(1)−O(1)−T(2)	134.3(4)	134.5(4)	135.3(6)	136.4(6)
T(1)−O(2)−T(2)	140.0(4)	146.2(3)	138.8(6)	138.4(5)
T(1)−O(3)−T(2)	138.7(4)	138.6(5)	135.3(7)	133.4(6)
T(1)−O(4)−T(2)	153.5(4)	150.3(4)	148.7(6)	147.7(6)
⟨T(1)−O−T(2)⟩				

Table 7. Selected Interatomic Silver Distances (Å) Derived from Fully Silver-Exchanged Faujasites with Standard Uncertainties in Parentheses

atoms	Ag−Y-450	Ag−X-450	Ag−LSX-350	Ag−LSX-450
Ag(I)−O(3)	2.649(4)	2.682(5)	2.583(7)	2.554(7)
Ag(I′)−O(3)	2.321(9)	2.30(1)	2.369(11)	2.393(11)
Ag(I′b)−O(3)		2.181(6)		
Ag(I)−Ag(I′)		2.36(2)	2.66(2)	2.79(2)
Ag(II′)−O(2)	2.670(3)			
Ag(II)−O(2)	2.335(5)	2.312(5)	2.206(7)	2.197(8)
Ag(II*)−O(2)		2.51(3)	2.43(4)	2.56(4)
Ag(III)−O(1)		2.77(5)	2.62(7)	2.71(6)
Ag(III)−O(4)		2.58(5)	2.75(5)	2.77(5)
Ag(III)−O(4)		2.61(5)	2.75(5)	2.80(5)

Table 8. Reported Site Occupancies for Silver-Exchanged Faujasites in Units of Silver/Unit Cell

atom	Ag−Y-450	Ag−X-450	Ag−LSX-350	Ag−LSX-450
I	10.9	1.9	8.5	8.5
I′	12.4	14.0	23.4	23.0
I′b		13.9		
II′	4.5			
II	27.5	25.8	25.3	25.0
II*		6.2	6.7	7.0
III		13.4	19.2	20.2
Ag found	55.3	75.2	83.1	83.7
Ag predicted	56	86	96	96

$= y = z$), or positional disorder along this axis. Models incorporating anistropic displacement parameters did not yield stable refinements. Furthermore, the Ag(I)−Ag(I′) distances of ≈1.87 Å are too short for either Ag^+−Ag^0 or Ag^+−Ag^+ bonds (Ag^0 = 1.44 Å; $Ag^+_{2coordinate}$ = 0.81 Å; $Ag^+_{4coordinate}$ = 1.14 Å).[26] The addition of a second silver site near the face of the hexagonal prism (referred to as I′b, see Figure 8) not only improves the fit and refines well but also is consistent with the presence of silver clusters. With the I′b site present, site I′ shifts 2.36 Å away from site I. There are two possibilities for silver−silver bonding. Although the distance between I and I′ is short, 2.36 Å, it is physically possible. A more plausible explanation is a bond between silver I′b atoms on opposite sides of the hexagonal prism, I′b−I′b = 2.64 Å. In this scenario, site I would be occupied 12% of the time, both I′ sites would be simultaneously occupied 44% of the time, and the I′b sites would be simultaneously occupied for the remainder.

There is no silver associated with the single six-ring and inside the sodalite cage (II′). The silver in SII, like that of the Ag−Y, is approximately in the plane of the six-ring. A new site, labeled II* to distinguish it from the conventional site II (see Figure 8), was located in this sample. Site II* is still observed on the supercage side of the six-ring, but is shifted further away from the plane of the six-ring. Similar to Ag−Y, the total occupancy of sites II and II* refined to slightly larger than unity. However, simultaneous occupancy at these sites is not possible because of their close proximity (II−II* = 0.75 Å), so their total occupancies were constrained to unity. Most of the cations (81%) were on the SII site. One explanation for the increase in distance between Ag(II*) and the six-ring is the presence of extraframework $[AlO_4]^-$ in the center of the sodalite cage. The agreement between the fractional occupancies of Ag(II*) (19%) and aluminate (18%) supports this argument. Unless there is a significant loss of oxygen at a particular site, it is doubtful that one can see much of an effect with neutron diffraction. One can treat such an effect by looking at the fractional occupancy of the framework, but in this case, the amounts are too small to see an effect. Furthermore, one will not see specific distortions (unless they happen to a specific site an appreciable number of times) because this is a technique by which we are looking at the average structure.

This model does not account for all the silver seen either by direct chemical analysis or by charge balance

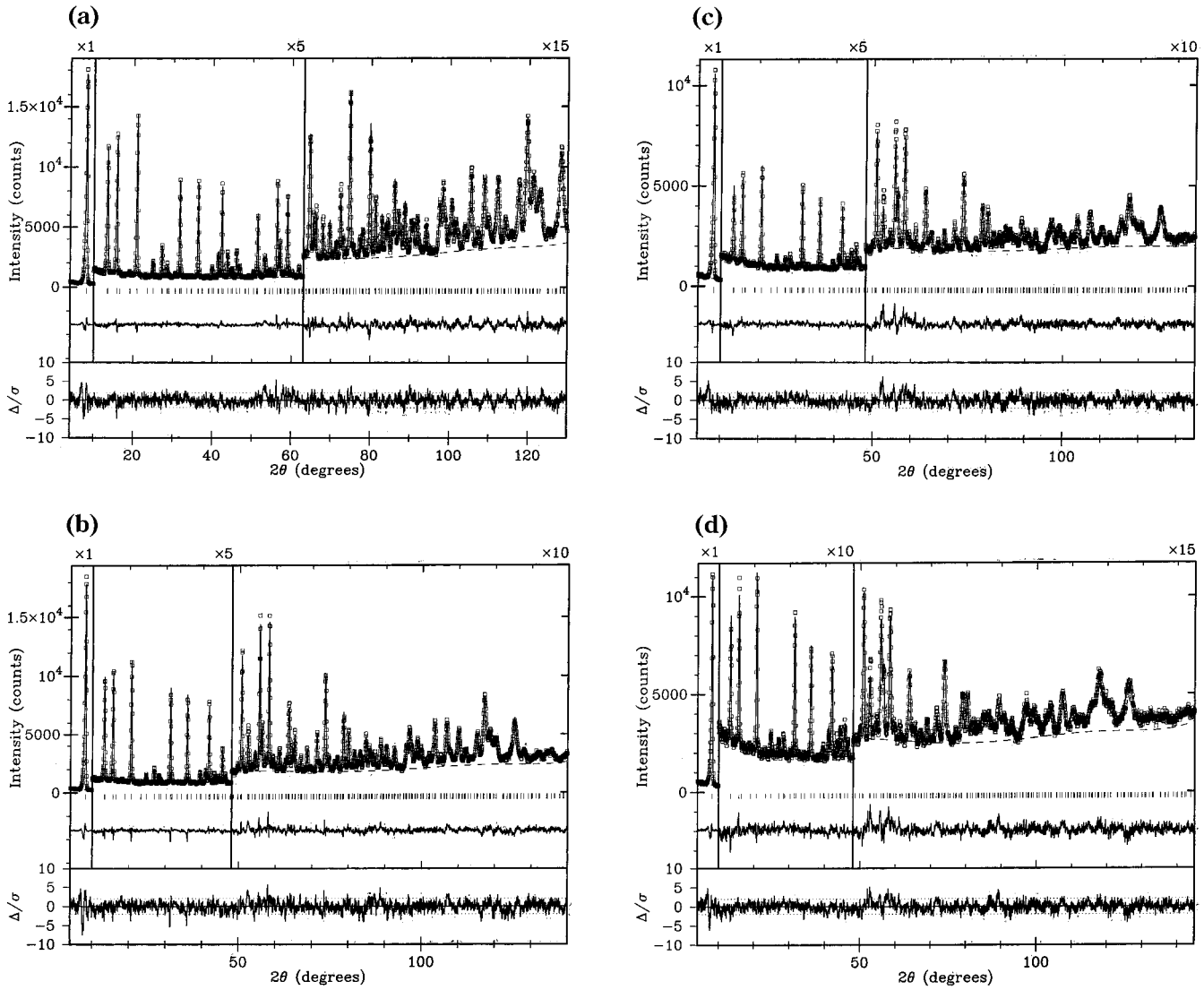

Figure 7. Computed and observed diffraction data (upper line and crosses, respectively) for the results of the Rietveld refinement of the structure of (a) Ag−Y, (b) Ag−X-450, (c) Ag−350-LSX, and (d) Ag−450-LSX using neutron powder diffraction data. The tic marks indicate the positions of reflections. The middle curve shows the difference between the observed and computed data and the lower curve shows the same differences, but weighted by the standard uncertainties. Sections of the plots are enlarged to better show details. The magnification factor is shown along the top axis of the graph.

considerations, although the discrepancy is not large considering the experimental error. In fact, the discrepancy between the Ag and Al chemical analyses is likely an indication of the presence of silver in a nonzeolitic phase.[14]

Ag−LSX-350 and Ag−LSX-450. The Ag−X model was used as the starting point for both Ag−LSX samples; however, positions of cations near the hexagonal prism (I and I′) were better described by the model developed for Ag−Y. There is evidence for significant disorder in the siting of silver along the (111) axis. We attribute this to differences in silver siting at the microscopic level. Indeed, several plausible models were found for the extraframework positions with minor variations in position and fractional occupancy for silver in the vicinity of the single six-ring and the hexagonal prism. The models we present below, in addition to being the simplest for these systems, also provide the best fit to the data and are stable with respect to refinement. It is important to note that models based on diffraction experiments represent an average structure. In reality, the chemical environment near each of these cationic positions may vary from unit cell to unit cell.

Like Ag−X, these materials had a strong gold coloration after vacuum dehydration, indicating the presence of silver clusters. For sites I and I′, the approximate occupancies are ≈50 and ≈70%, respectively. This requires that sites I and I′ must, at times, be simultaneously occupied. The I−I′ distances, 2.66 and 2.79 Å in Ag−350-LSX and Ag−350-LSX are consistent with silver−silver interactions. The data do not allow us to further define the nature of the silver clustering.

Similar to Ag−X, the silver at the single six-ring resides in sites II and II*. As before, the total occupancy of these sites tended to refine to greater than unity, and so, they were appropriately constrained. For Ag−350-LSX, it is possible to attribute this silver distribution to the presence of extraframework aluminate in the sodalite cage, as the fractional occupancies of these two sites are nearly identical. In Ag−450-LSX, the correlation between the fractional occupancies of extraframework species in site II* (27%) and the aluminate site

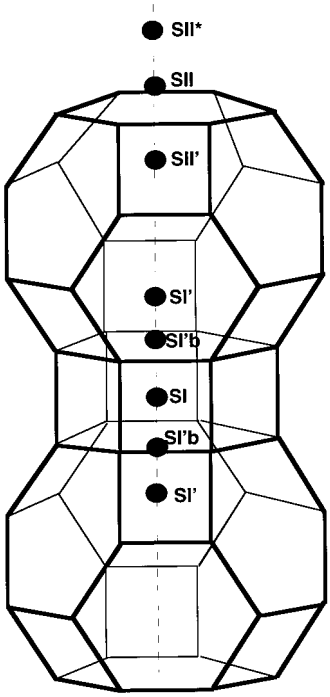

Figure 8. The position of extraframework sites in relationship to the sodalite cage in the faujasite structure.

(38%) is less obvious. A significantly improved fit was obtained by removing the soft constraint on the Al−O distance in the extraframework aluminate for Ag−450-LSX. This was not true for Ag−X or Ag−350-LSX. Relative to the expected 1.73 Å, the bond length was 1.93 Å. We interpret the lengthening of the Al−O distance and the increased scattering from the sodalite cage site to the presence of other species occluded in the sodalite cage. The data are insufficient to justify a more complex model. There is a definite effect on the adsorptive capacity that is related to the temperature of dehydration/activation. Cation migration in zeolites is usually the result of energetic instabilities within the framework (i.e., the cations move to lower their energy, to satisfy their coordination requirements). In this case, we believe that the breakdown of the framework results in an energetically unfavorable environment within the beta cage (sodalite cage). This encourages migration of Ag from the conventional SII location to the novel and more adsorbate accessible SII* location.

Both models are slightly silver deficient relative to the amount of silver required by charge balance and are significantly below the direct chemical analysis for silver. The former is likely due to the disorder in silver siting while the latter provides a strong argument for the presence of silver in nonzeolitic form.

Bond Valence Calculations. The concept of bond valence is particularly useful for understanding the relative strength of an interaction between a cation and an anion. When a cation is close to the framework, its interaction is with the framework oxygen atoms, which will be relatively strong, and it is less likely to interact with other species because its coordination requirements are being satisfied by the framework. This corresponds to a situation where the valence number of silver would approach a value of 1, the formal oxidation state of extraframework silver. As Ag^+ moves away from the framework, its coordination environment becomes relatively unsaturated because the Coulombic interactions between silver and the framework oxygen decrease to reflect the fact that its coordination requirements are no longer being completely satisfied. A valence number significantly below unity indicates that silver is coordinatively unsaturated and provides a likely site for N_2 adsorption.

Table 9. Calculated Valence Number (V_{Ag}) for Silver Cations Residing in the Supercage

atom	Ag−Y-450	Ag−X-450	Ag−LSX-350	Ag−LSX-450
II	0.88	0.89	1.12	1.14
II*		0.56	0.68	0.46
III		0.41	0.34	0.29

For these calculations, the valence number, v_{ij}, of a bond between two atoms i and j is defined such that the sum of all of the valences from a given atom i with valence V_i obeys

$$V_i = \sum_j v_{ij} \tag{3}$$

The expression for determining the valence number of a particular atom based on experimentally derived bond distances is

$$v_{ij} = \exp[R_{ij}(-d_{ij})/b] \tag{4}$$

where d_{ij} is the measured bond distance, R_{ij} is the derived bond valence parameter,[27] and b is a constant equal to 0.37 Å.[28]

The valence number of silver in sites II, II*, and III are listed in Table 9. These silver sites were chosen because they are accessible to potential adsorbates. The value for R_{ij}, 1.805 Å, was taken from ref 27. Silver−oxygen interactions of up to 4 Å were included in the calculation; each Ag−O interaction >4 Å will contribute <0.003 to the total calculated valence number and was thus ignored.

Site II cations for all the zeolites are effectively coordinated by framework oxygen atoms. The values in LSX are unusually high, but would drop to unity with small displacements from their current sites. This gives further evidence that disorder occurs, which cannot be modeled crystallographically.

The relatively large displacement of the cation from the six-ring in Ag−X, Ag−350-LSX, and Ag−LSX-450 leads to much lower bond valence numbers, 0.58, 0.68, and 0.46, respectively. Furthermore, the displacement of the cation from the six-ring leaves it available for interactions with adsorbate molecules with less steric repulsion from the framework.

The silver cations at site III have lower valence numbers than any other cations in silver-exchanged faujasites. The extremely low bond valence numbers are indicative of little interaction between Ag(III) and the framework oxygen. These cations are exposed because they are sterically unencumbered. The exposed nature of all cations at site III, as well as that of site II* cations in Ag−X and Ag−450-LSX, makes them available to interact with adsorbate molecules such as N_2.

Model for the Adsorption of Nitrogen by Ag-Exchanged Faujasites. Several features of the N_2 adsorption isotherms shown in Figures 2, 4, and 5 merit

(27) Brese, N. E.; O'Keefe, M. *Acta Crystallogr.* **1991**, *B47*, 192.
(28) Brown, I. D.; Altermatt, D. *Acta Crystallogr.* **1985**, *B41*, 244.

further consideration. The adsorption of N_2 on Ag−Y is quite low. The Ag−X sample had a higher N_2 adsorptive capacity than that of Ag−Y, but showed little increase in adsorption with heat treatment at 450 °C relative to Ag−X that had been heat treated at 350 °C. Furthermore, the sample did not appear to be sensitive to heating in air. The N_2 adsorptive capacity for the Ag−LSX sample increased when dehydrated at 450 °C relative to a sample that was dehydrated at 350 °C. Ag−LSX proved to be sensitive to heating in air and even had a reduced adsorption capacity when initially dried in air at 100 °C before being fully dehydrated in a vacuum. This material was especially sensitive to heating to dehydration temperatures (350 °C and higher) in air.

Adsorbate−zeolite interactions correspond to those of the adsorbing gas with the surface oxygen and charge-compensating cations. Because the aluminum and silicon are tetrahedrally coordinated and well shielded,[29] their interactions with the adsorbate gas atoms can be neglected.[1] In zeolites with the faujasite structure, cations in the sodalite cages and the double six-ring (hexagonal prism) are sterically inaccessible to nitrogen and do not interact. Therefore, only the supercage (II, II*, and III) cations can interact with the adsorbate gas. The electric field around the supercage cations is affected by the shielding from the surrounding oxygen atoms. Because of this shielding, the electrostatic and induction interactions are expected to be lower than that of an isolated ion. Furthermore, the dispersion forces acting on the molecule will be larger because adsorbate molecules also interact with oxygen atoms of the zeolite. Therefore, the further a cation sits from the surface of the zeolite framework, the greater its interaction with an adsorbate molecule will be.

The calculated valence numbers for supercage silver cations provide a means of quantifying the strength of the Ag^+-N_2 interaction that results in the observed adsorption isotherms. The number of silver cations in a particular site and the magnitude of the silver valence should correlate directly with the adsorptive capacity of these zeolites.

The high valence number of the supercage Ag^+ in silver Y indicates that the extraframework cations are coordinately saturated and, therefore, are expected to have a relatively small interaction with N_2. This is consistent with the relatively low adsorptive capacity of Ag−Y (Figure 2d). In contrast, Ag−X and Ag−LSX have higher adsorptive capacities increasing from Ag−X to Ag−350-LSX to Ag−450-LSX. The relatively low valence numbers for Ag^+ in these materials for Ag^+ at sites II* and III indicate that these sites are relatively exposed. This exposure leads to a higher electrical field at these sites. That, coupled with the small amount of N_2-Ag^+ π-complexation, acts to increase the adsorption of N_2 for these zeolites. Although site II* is exposed in these materials, site III cations have the lowest valence for Ag^+ and are the primary contributor to N_2 adsorption. The decreasing value for the valence of site III is consistent with the enhanced adsorption of N_2 by Ag−X, Ag−350-LSX, and Ag−450-LSX, respectively (Figure 2b−d). The Ag−LSX-450 sample had a higher N_2 adsorptive capacity than that of the Ag−LSX-350 sample. However, the population of SIII cations for these samples is nearly the same. Therefore, this boost in the N_2 adsorption capacity is a result of a combination of a slightly lower valence number for the SIII cations and a larger population of SII* cations that also have a much lower valence number.

In Figure 4, the adsorptive capacity of Ag−350-LSX and Ag−450-LSX (dried at room temperature and dehydrated under vacuum at the specified temperatures) are compared to samples that were initially dried at higher temperatures. It is obvious that drying samples above room temperature in air, not vacuum, causes degradation of the adsorptive capacity. We believe that this decrease in adsorptive capacity arises from structural degradation of the LSX framework. Neutron powder diffraction data were collected for the sample that had been dried in air at 100 °C, dehydrated in air at 450 °C for 12 h, and finally dehydrated under vacuum at 450 °C (Figure 4d). Diffraction data indicated that this sample was practically amorphous, with only the (111) Bragg diffraction peak observed. The loss of crystallinity in this sample explains the low N_2 adsorption. Samples that had been vacuum dehydrated at temperatures above 500 °C also showed a decline in the adsorptive capacity that may also be attributed to sample degradation.

Structural degradation is also consistent with the only small decrease in adsorptive capacity in Ag−X upon heating in air. Structural degradation in faujasites arises from their tendency to lose framework alumina through self-steaming to void spaces in the zeolite. This tendency is most pronounced in LSX, although it also occurs in X. The adsorption isotherms in Figure 5 are consistent with only mild degradation of Ag−X from drying at 100 °C followed by vacuum dehydration at 350 °C relative to drying at 25 °C followed by vacuum dehydration at 450 °C.

The presence of cations with varying levels of framework interaction results in an energetically heterogeneous adsorptive surface. Energetic heterogeneity in zeolites results when there are local intracrystalline sites where guest molecules are preferentially sorbed more exothermally than in the rest of the intracrystalline volume. This is due to a combination of cations in very different coordination environments and to high-energy cations in sites with low shielding.

The presence of energetic heterogeneity of a system can be determined by comparing the isosteric heat of adsorption of N_2 to the amount of N_2 adsorbed. Energetic heterogeneity in the system will result in a decrease of the isosteric heat of adsorption as the amount of N_2 adsorbed increases. For small uptakes, the isosteric heat may decrease rather strongly with the amount adsorbed. At intermediate uptakes, the slope of this plot will usually decrease and become nearly horizontal.

When adsorption isotherms at different temperatures are measured, the heat of adsorption as a function of

(29) Coe, C. G. In *Access in Nanoporous Materials*; Pinnavaia, T. J., Thorpe, M. F., Eds.; Plenum Press: New York, 1995; p 213.
(30) Wagner, C. D., Riggs, W. M., Davis, L. E., Moulder, J. F., Mullenberg, G. E., Eds.; *Handbook of X-ray Photoelectron Spectroscopy*; Perkin-Elmer Corp.: Eden Prairie, MN, 1979.
(31) Gaarenstroom, S. W.; Winograd, N. *J. Chem. Phys.* **1977**, *67*, 3500.
(32) Freeman, C. M.; Catlow, C. R. A.; Thomas, J. M.; Brode, S. *Chem. Phys. Lett.* **1991**, *186*, 137.

surface coverage can be calculated through application of the Clausius−Claperyron equation as follows:

$$\Delta H_{ads} = R\left(\frac{d \ln P}{d(1/T)}\right)_n \quad (5)$$

When the data from adsorption isotherms measured at 50, 25, and 0 °C are used, the isosteric heats of adsorption for N_2 on Ag−LSX (vacuum dehydrated at 450 °C) and Li−LSX (Li^+ ion-exchanged LSX zeolite) were determined by evaluating the slope of a plot of ln(P) versus (1/T) at several levels of N_2 coverages (Figure 9). This plot shows a high initial heat of adsorption for Ag−LSX-450 that initially drops quickly and then gradually becomes nearly horizontal at high adsorbate coverage. This indicates the presence of sites where the adsorbate is preferentially adsorbed more exothermally than at others. This is consistent with the presence of two sites (III and II*), which are capable of interacting with N_2. Initially, the cations with the poorest coordination environments will adsorb N_2 (III). This will be a more exothermic process because N_2 adsorption greatly improves their coordination environment. As these sites are filled, sites with slightly better coordination (III and II*) will adsorb N_2. By comparison, the heat of adsorption for N_2 on Li−LSX is also shown. Relative to Ag−LSX-450, this is an energetically homogeneous adsorptive surface; the heat of adsorption data indicate the presence of only a single adsorptive site. In Li−LSX, Li^+ ions in site II are well coordinated and have little, if any, interaction with N_2. Only Li in SIII interact with the N_2.[8,29]

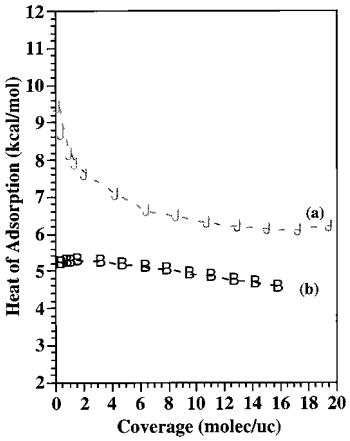

Figure 9. Heat of adsorption (kcal/mol) versus surface coverage (molecules/unit cell) for N_2 adsorption on (a) Ag−LSX-450 and (b) Li−LSX-450.

Conclusions

The adsorptive capacity of silver ion-exchanged faujasites is affected by the specific conditions under which they are dehydrated. Low-silica X zeolites are especially sensitive to the dehydration conditions. Silver ion-exchanged Y zeolites had a low capacity for nitrogen adsorption due to a lack of easily accessible supercage cations. Silver ion-exchanged X zeolite had a much higher nitrogen adsorption capacity as expected because it contains readily accessible supercage cations in site III locations. However, the Ag−X zeolite did not show enhancement of the nitrogen adsorption with dehydration temperatures above 350 °C. The silver ion-exchanged low-silica X zeolites had a high nitrogen adsorption capacity, which was enhanced with the presence of coordinatively unsaturated silver cations in site II* locations. Silver in this location is more easily accessible to the sorbate molecules than those in the more usual site II locations near the single six-ring. The presence of these site II* cations seems to be affected by the dehydration temperature with the Ag−LSX-350 sample containing fewer SII* cations (and with a higher valence number) than that of the Ag−LSX-450 sample. These SII* cations seems to be the result of thermally induced cation and/or cluster migration from cations near the single six-ring due to the formation of an extraframework phase in the center of the sodalite cage. We have modeled this extraframework phase as alumina.

Acknowledgment. This work was supported by the U.S. Department of Energy under Grant DE-FG26-98FT40115 and National Science Foundation. Neutron activation analyses (NAA) were conducted in the Ford Nuclear Reactor of the Phoenix Memorial Laboratory at the University of Michigan. Leah Minc of the Michigan Memorial Phoenix Project coordinated the analyses. X-ray photoemission spectroscopy was conducted using the instrumentation in the University of Michigan's Electron Microscopy Analysis Laboratory (EMAL). Stefan Zajic, a visiting undergraduate student from the University of Pennsylvania, assisted in the synthesis of the Ag−zeolites.

Certain trade names and company products are identified to adequately specify experimental procedures. Such identification does not imply recommendation or endorsement by the National Institute of Standards and Technology, nor does it imply that the products are necessarily the best available for the purpose.

CM000294N